THE JOURNAL OF PHYSICAL CHEMISTRY B

Article

pubs.acs.org/JPCB

Structure of Molten $CaSiO_3$: Neutron Diffraction Isotope Substitution with Aerodynamic Levitation and Molecular Dynamics Study

L. B. Skinner,[†,*] C. J. Benmore,[‡] J. K. R. Weber,[‡,§] S. Tumber,[§] L. Lazareva,[†] J. Neuefeind,[⊥] L. Santodonato,[⊥] J. Du,[∥] and J. B. Parise[†,○]

[†]Mineral Physics Institute & Department of Geosciences, Stony Brook University, Stony Brook, New York 11794-2100, United States

[‡]X-ray Science Division, Advanced Photon Source, Argonne National Laboratory, Argonne, Illinois 60439, United States

[§]Materials Development, Inc., Arlington Heights, Illinois 60004, United States

[⊥]Spallation Neutron Source, Oak Ridge National Laboratory, Oak Ridge, Tennessee, United States

[∥]Dept. of Material Science and Engineering, University of North Texas, Denton, Texas 76203, United States

[○]Light Source Division, Brookhaven National Laboratory, Upton, New York 11973, United States

ABSTRACT: We have performed neutron diffraction isotopic substitution experiments on aerodynamically levitated droplets of $CaSiO_3$, to directly extract intermediate and local structural information on the Ca environment. The results show a substantial broadening of the first Ca−O peak in the pair distribution function of the melt compared to the glass, which comprises primarily of 6- and 7-fold coordinated Ca-polyhedra. The broadening can be explained by a redistribution of Ca−O bond lengths, especially toward longer distances in the liquid. The first order neutron difference function provides a test of recent molecular dynamics simulations and supports the MD model which contains short chains or channels of edge shared Ca-octahedra in the liquid state. It is suggested that the polymerization of Ca-polyhedra is responsible for the fragile viscosity behavior of the melt and the glass forming ability in $CaSiO_3$.

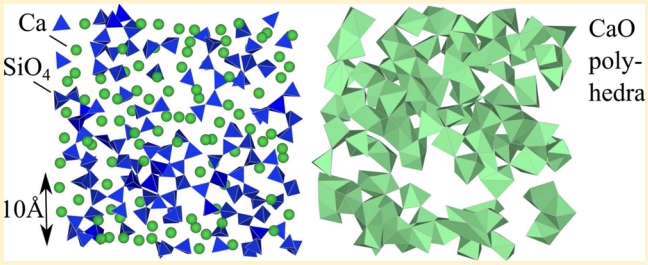

1. INTRODUCTION

The local and intermediate range structure of high temperature silicate melts has been of long-standing interest in geophysics and glass science, due to the effect on viscosity and thermodynamic properties.[1−6] Calcium silicate glasses in particular have often been used as a benchmark system for testing theories of modifier ordering.[3−8] Silicate glasses are also studied for their significance in understanding the formation of the Earth's mantle and their role as a major component of soda-lime glass.[1,8] However, the accurate determination of liquid structure of silicate liquids is problematic due to the high temperatures needed. Although much progress has been made in recent years studying high temperature liquids using total X-ray and neutron scattering techniques combined with aerodynamic levitation,[9−12] the measured structure factors are inherently broad and comprise of several overlapping contributions making structural interpretations difficult. In this work we have directly measured the short and intermediate range calcium correlations in a $CaSiO_3$ melt by performing a first order difference neutron diffraction measurement using isotopic substitution on aerodynamically levitated droplets. The results reveal significant structural differences in the Ca cation environments between the liquid and glassy states, as predicted by recent molecular dynamics simulations,[13] indicating that temperature dependence needs to be taken into account in precise atomic models of high temperature liquids.[1,14]

In $CaSiO_3$ glass, the detailed structural arrangements of the Ca cation have previously been accurately determined from a double difference neutron diffraction (isotope substitution) experiment, showing that calcium silicate exhibits both well-defined local and intermediate range order.[3] This intermediate range order has been confirmed by molecular dynamics (MD) simulations, which predict a glassy tetrahedral silica network with short-range order similar to the crystal wollastonite, but no evidence of sheet arrangements were found.[8] Silicate liquids, however, possess both strong directional covalent bonding and partly ionic bonding that can change significantly with temperature.[1,2] Recent high-energy X-ray experiments and molecular dynamics simulations have shown that the Ca environment changes significantly for aluminates and silicates, between the high temperature liquid state and the quenched glass.[13,15] Using the intense flux of the Spallation Neutron Source, we have successfully measured the local and intermediate range structure associated with the Ca atoms in molten $CaSiO_3$ using calcium isotopic substitution and compared the results directly to that of the glass.

Received: July 3, 2012
Revised: September 18, 2012
Published: October 29, 2012

dx.doi.org/10.1021/jp3066019 | J. Phys. Chem. B 2012, 116, 13439−13447

2. THEORY

i. Isotope Difference Methods. Typically a single neutron diffraction experiment provides a measurement of the total differential cross section $I_N(Q)$ which is related to the total interference function $F_N(Q)$ by $I_N(Q) = F_N(Q)+C$ where C is a constant representing the incoherent and coherent self-scattering (see[16] for further detail). $F_N(Q)$ can then be deconstructed into a weighted linear combination of all the pairwise partial structure factors $S_{\alpha\beta}(Q)$.

$$F_N(Q) = \sum_{\alpha}\sum_{\beta} c_\alpha c_\beta b_\alpha b_\beta^* (S_{\alpha\beta}(Q) - 1) \quad (1)$$

Here α, β represent the chemical species in the sample, c_α is the concentration of species α, and b_α is the coherent scattering length of species α. Since $CaSiO_3$ is a three component system the structure can be reduced into six distinct pairwise structure factors, namely, CaCa, CaSi, CaO, SiSi, SiO, and OO. An advantage of the partially enriched ^{43}Ca isotope sample used here is that it has a near zero coherent neutron scattering length (0.38 fm). The weightings for this isotopic sample result in Si−O and O−O contributing over 90% of the total structure factor (complete weightings are given below, calculated from the tabulated values in ref 17).

$$\begin{aligned} {}^{iso}F_N(Q) = {} & 0.0059[S_{CaCa}(Q) - 1] + 0.1275 \\ & [S_{CaSi}(Q) - 1] + 0.5350[S_{CaO}(Q) - 1] \\ & +0.6892[S_{SiSi}(Q) - 1] + 5.7832[S_{SiO}(Q) - 1] \\ & + 12.1313[S_{OO}(Q) - 1] \end{aligned} \quad (2)$$

A difference measurement allows partial separation of these six structure factors. Here by using two samples with differing b_{Ca} a structure factor containing only Ca−Ca, Ca−Si, and Ca−O is obtained ($\Delta F_N(Q)$). For this difference experiment measurements were made on the empty nozzle, the natural liquid, the isotopic liquid, a vanadium ball, and a nickel calibration ball. The isotopically enriched glass was also measured for comparison purposes.

Formally the difference $\Delta F_N(Q)$ between the natural and isotope samples is

$$\begin{aligned} \Delta F_N(Q) = {} & {}^{nat}F_N(Q) - {}^{iso}F_N(Q) \\ = {} & c_{Ca}{}^2(b_{Ca}{}^2 - b_{Ca43}{}^2)[S_{CaCa}(Q) - 1] \\ & + 2c_{Ca}c_{Si}(b_{Ca} - b_{Ca43})b_{Si}[S_{CaSi}(Q) - 1] \\ & + 2c_{Ca}c_{O}(b_{Ca} - b_{Ca43})b_{o}[S_{CaO}(Q) - 1] \end{aligned} \quad (3)$$

This gives the following weightings:

$$\begin{aligned} \Delta F_N(Q) = {} & 0.877[S_{CaCa}(Q) - 1] + 1.431[S_{CaSi}(Q) - 1] \\ & + 6.013[S_{CaO}(Q) - 1] \end{aligned} \quad (4)$$

The real space pair distribution functions are given by the sine Fourier transforms of these structure factors. Specifically, $G_N(r)$, is defined as

$$G_N(r) - 1 = \frac{1}{2\pi^2 r\rho}\int_{Q_{min}}^{Q_{max}} \left(\frac{F_N(Q)}{w}\right) Q \sin(Qr)\, dQ \quad (5)$$

where $w = \Sigma_\alpha \Sigma_\beta c_\alpha c_\beta b_\alpha b_\beta$, and ρ is the number density of the sample in atoms per Å^3.

Also the $D_N(r)$ differential pair distribution function used is defined as:

$$D_N(r) = 4\pi\rho r[G_N(r) - 1] \quad (6)$$

The main difficulty in performing this type of experiment on high temperature aerodynamically levitated melts has been the accurate measurement of such a small neutron *difference* signal between two ~3 mm diameter droplets.[24] For example, the samples used in this experiment weighed ~45 mg each.

3. EXPERIMENTAL AND SIMULATION DETAILS

The neutron experiments were performed on the high-intensity Nanoscale Ordered Materials Diffractometer (NOMAD) at the Spallation Neutron Source, Oak Ridge National Laboratory, USA. An aerodynamic levitator was used to suspend the samples, in an upward flow of 99.999% purity argon, while they were melted with a 240 W carbon dioxide laser (Evolution 240, Synrad, Inc., Mukilteo, WA[25]). Alignment of the sample in a circular, 5 mm diameter neutron beam was performed using a neutron camera. An optical pyrometer (Chino IR-GZ01R) was used to measure the apparent surface temperature of the heated droplets. A spectral emissivity correction was applied to this using a value of 0.92.[18] During data collection, the natural and isotope liquids were held at a temperature of 1650 ± 100 °C for 3 h (the melting temperature of $CaSiO_3$ is 1540 °C).

i. Aerodynamic Levitation. The container-less sample environment used here enabled this high temperature experiment by (i) eliminating container-derived sample contamination, and (ii) minimizing container scattering. The layout of the aerodynamic levitator on the NOMAD instrument is illustrated in Figure 1.

The levitator components were arranged inside a sample well that was fabricated from a thin-walled aluminum cylinder. The neutron beam entered the chamber through a thin vanadium

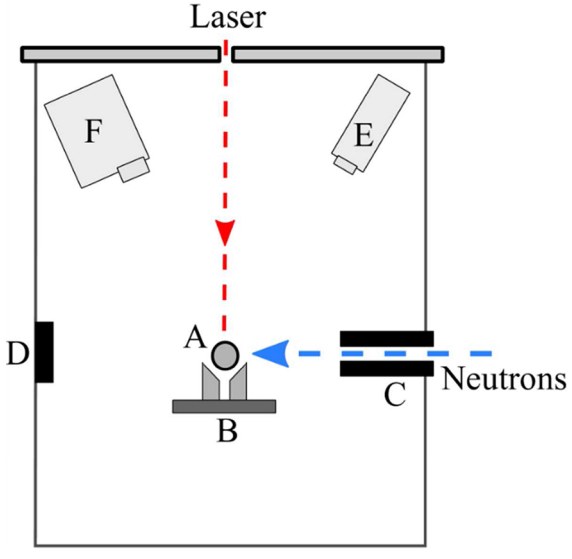

Figure 1. Layout of the beamline levitator components within the sample well at the NOMAD instrument (beamline B1B), SNS. The laser heated, aerodynamically levitated sample (A), was floated above a vanadium nozzle (B) which was water cooled and mounted on an XY stage. The incident neutron beam was collimated by a boron nitride tube (C). Unscattered neutrons were absorbed behind the sample by a boron carbide block (D). The sample was monitored by a video camera (E) and optical pyrometer (F).

dx.doi.org/10.1021/jp3066019 | J. Phys. Chem. B 2012, 116, 13439−13447

window, then passed through a circular beam-defining boron nitride tube. The downstream port was covered with a 20 mm thick boron carbide absorber which covered the vanadium window. The levitator comprised a solid vanadium nozzle with a cone-shaped 90° opening angle, and a 0.7 mm diameter gas-flow hole. The nozzle was housed in a water-cooled mounting that was secured to an X−Y stage. The stage was supported from the chamber lid with a rigid aluminum rod. This rod was also used to mount an optical pyrometer, video camera and a laser beam-focusing lens. The pyrometer alignment was checked remotely from a video camera mounted onto the eyepiece (this setup is also detailed in Figure 1).

Once the system was installed, a solid nickel test ball was placed in the levitation nozzle. A neutron sensitive camera was mounted downstream of the nozzle and the neutron beam was used to search for the shadow formed from absorption by the sample. The X−Y position and height of the nozzle were adjusted to locate the sample in the axis of the incoming neutron beam. The beamline detector vessel was then evacuated and the sample well was purged by flowing 99.999% purity argon through the levitation nozzle. The CO_2 heating laser was then precisely aligned with the levitated sample using a visible wavelength tracer beam. The sample was levitated using a flow of 200−500 cm^3/min of argon. The levitator controls were operated remotely using a *LabVIEW* program.

On the basis of the temperature versus time measurement the average natural sample temperature was 1650 °C and the average isotope sample was 1675 °C, both measurements exhibited fluctuations of <50 °C.

ii. Nanoscale Ordered MAterials neutron Diffractometer. The NOMAD instrument and data reduction procedure have recently been described in ref 25. For our data reduction only the low angle ^{3}He position sensitive detector banks[19] were used as backscattering from the boron nitride collimator resulted in large backgrounds in the high angle banks. The exact scattering angle of all detector pixels was calibrated by placing a 3 mm Cu-bead in the levitator nozzle at the sample position. All measured neutron intensities were normalized to the proton charge on the target. Normalization to the differential cross section was accomplished with reference to both a 3 mm diameter vanadium ball and the measured flux in the upstream beam monitor (see ref 25 for further detail). Angular and energy dependence of multiple scattering and absorption corrections were not applied as they are expected to be minimal, given the small sample volume and cross sections of this measurement.[8]

iii. Isotope Breakdown and Microprobe Analysis. The isotopic sample was partially enriched with ^{43}Ca. The actual breakdown is given in Table 1.

Table 1. Atomic Percentages of the Enriched Ca Isotope Sample

isotope	atomic %
Ca-40	23.8
Ca-42	1.00
Ca-43	62.2(±0.3)
Ca-44	12.8
Ca-46	<0.01
Ca-48	0.2

Using scattering lengths from ref 17 gives a coherent neutron scattering length of: 0.38(3) fm for the b_{Ca} of the isotope sample, vs 4.70(2) for the natural sample of the same composition. The $CaSiO_3$ composition samples were made from mixtures of high purity $CaCO_3$ (99.95%) and SiO_2 (99.995%) that were ground, mixed, calcined, and then fused into roughly spherical pieces using a laser hearth.[10] After 3 h of high temperature levitation, the natural and isotope samples were recovered as glasses, and found to have lost approximately 10% of their respective starting mass.

The recovered natural glass bead composition was analyzed with a JEOL JXA 8200 electron microprobe at the Institute of Meteoritics (University of New Mexico). The analyses were conducted using an accelerating voltage of 15 kV and a beam current of 20 nA. A 10 μm diameter beam was used for each glass analysis. The Ca and Si peaks were counted for 30 s while the backgrounds were counted for 15 s. Diopside ($MgCaSi_2O_6$) was used as the standard for Si and wollastonite ($CaSiO_3$) was used as the standard for Ca. The composition of the recovered natural glass bead was found to be 46.45 wt % SiO_2 and 53.55 wt % CaO. This is the average of 340 measurement points which had a standard deviation of 0.17 wt %. These values were obtained after rescaling the data such that the total added up to 100%, not the 100.71% of the raw data, and this 0.71 wt % was used as an approximate upper limit on the systematic error present in the composition measurement.

iv. X-ray Diffraction Measurements. High energy X-ray diffraction measurements were performed on the recovered glass beads from the neutron experiment. Since X-rays are essentially insensitive to the isotopic change between samples, the data taken on beamline 11-ID-C of the Advanced Photon Source, confirms the natural and isotopic $CaSiO_3$ samples were structurally identical. The recovered glass samples were placed on ∼10micrometer thick kapton tape, and illuminated with 0.10803(1) Å, X-rays. The diffraction patterns were collected with a Perkin-Elmer amorphous silicon area detector (XRD1621) perpendicular to the incident beam, and 457.0(5) mm downstream from the sample position. The instrument was calibrated using a CeO_2 powder standard, and the data was reduced using the *Fit2D* program.[27] The isotopic sample pattern was scaled by 0.955, to match the high-Q scattering level of the natural measurement (see Figure 2a). This rescaling is effectively correcting for scattering volume and incident flux variation between the two measurements. These raw intensities plotted in Figure 2a) include air scattering, kapton scattering, and Compton scattering, in addition to the X-ray structure factor of the samples. The measured X-ray principal peak positions differed by 0.4%, and principal peak heights differed by 1.5% between the natural and isotopic samples (Figure 2b).

The real space X-ray difference $\Delta G_X(r)$ shows very small opposing differences in the SiO_2 and CaO first coordination shells (see Figure 2b). This small difference is consistent with the final sample compositions being 1.4 wt % different, and with the isotopic sample having lost less SiO_2 than the 3.55 wt % lost by the natural sample. This composition change is also consistent with the observation that the isotopic sample lost less mass than the natural sample. The 1.4 wt % difference gives a similar change in the partial structure factor weightings of the difference function. These differences in the X-ray spectra do not affect the conclusions of this work for the following reasons: (i) The 1.4 wt % difference is less than the ∼3.55 wt % compositional drift from start to finish of the neutron

dx.doi.org/10.1021/jp3066019 | J. Phys. Chem. B 2012, 116, 13439−13447

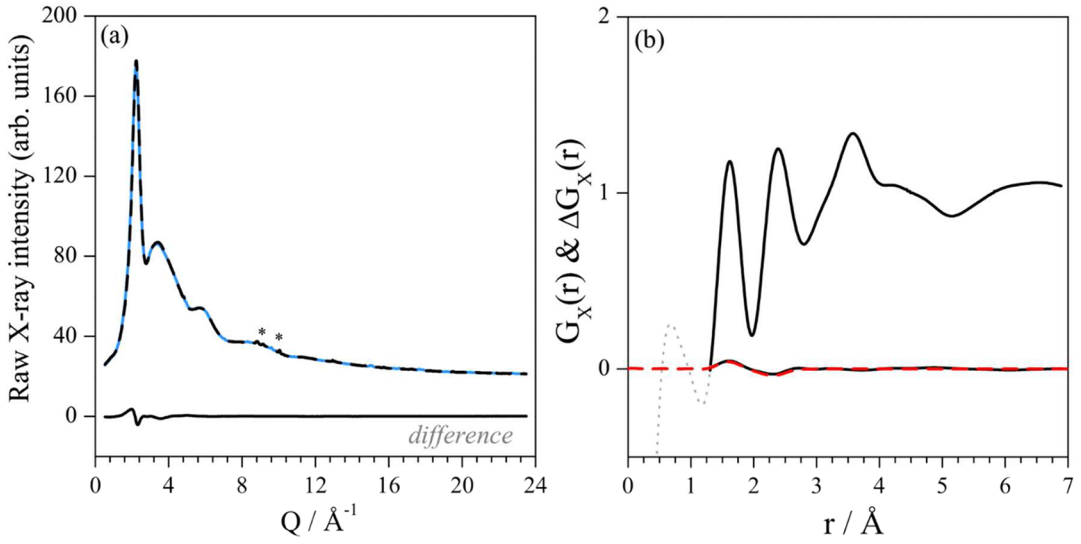

Figure 2. (a) Raw measured X-ray intensity. The natural sample (black dashed line) and isotope sample (blue solid line). The lower black line is the difference between the isotope and natural samples. The small Bragg peaks denoted by ∗ are memory effects in the detector, not the sample, as evidenced by their movement with detector position and the fact that they exactly cancel in the difference pattern (see ref 28 for further detail). (b) The upper black line is the measured X-ray $g(r)$ and the lower black line is the transform of the difference function. Both were transformed with a Lorch modification using Q_{max} = 15 Å^{-1}. The gray dotted line is the unphysical low-r part of the measured $G_X(r)$. The red dashed line is a peak fit corresponding to 1.4 wt % SiO_2 excess and a 1.4 wt % CaO deficiency.

experiment. (ii) It contributes less error than the uncertainty in the neutron scattering length values. (iii) The 1.4 wt % is also the maximum difference at any given time during the run (since the natural and isotopically enriched samples had the same starting composition). For example, assuming a constant rate of loss, gives a mean difference of 0.7 wt % during the measurement. (iv) The neutron real space difference shows no significant Si−O peak at 1.6 Å, which is a strong consistency check that the natural and isotopically enriched $CaSiO_3$ samples were essentially the same.

v. MD Simulation Details. A simulation box totalling 6400 atoms, giving an approximate box side length of 45 Å was performed using previously published pair potentials.[13] To overcome the short-range attraction in the buckingham potentials, an r^{-12} term was added to correct the short-range attraction, while leaving r > 1 Å unchanged. The constant $D_{\alpha\beta}$ was chosen such that the derivative of the potential was always positive at low-r, ensuring short-range repulsion (Table 2).

$$U_{\alpha\beta}(r) = \frac{q_\alpha q_\beta}{r} + A_{\alpha\beta}\exp(-r/B_{\alpha\beta}) - \frac{C_{\alpha\beta}}{r^6} + \frac{D_{\alpha\beta}}{r^{12}} \quad (7)$$

The metal−metal interactions contain only the coulomb repulsion. Prior to starting the simulation the atoms were separated to a minimum of 75% of their expected bond lengths. The simulation was initially equilibriated at 6000 K for 50 ps (*NPT*), then brought to 2000 K for 150 ps (NPT). The temperature was then dropped in 50 K intervals every 100 ps, down to 1000 K (which is below the glass transition temperature). The liquid structure was taken from averaging over the second half of the 1950 K run. For the room temperature glass, the temperature was dropped from 1000 K to 300 K and run for a further 100 ps, before structures were averaged from a final 50 ps run. This procedure provided an effective cooling rate of ∼5 × 10^{11} K/s, compared to the ∼5 × 10^2 K/s experimental cooling rate. This difference in cooling rate is expected to produce a simulated glass structure with a higher fictive temperature than the experimental glass, and it may explain some of the slight disagreements between the simulated and measured glass structures.

Table 2. MD Potential Parameters Used in the Simulation[a]

pair	A/eV	B/Å	C/Å^6	D/Å^{12}
$Ca^{1.2}O^{-1.2}$	7747.1834	0.252 623	93.109	12
$Si^{2.4}O^{-1.2}$	1302.905	0.193 817	54.681	2.2
$Al^{1.8}O^{-1.2}$	12201.42	0.1956	32	1.0
$O^{-1.2}O^{-1.2}$	2029.2204	0.343 645	192.58	200

[a]Note that Si−Si, Ca−Ca, and Al−Al interactions were governed by charge repulsion only.

vi. Sample Density. The measured glass density for $CaSiO_3$ is 0.074 ± 0.001 atoms Å^{-3} and the MD simulation of the glass agrees with this value. For the liquid number density we used 0.067 Å^{-3} obtained from the temperature-density variation of the MD simulation. Figure 3 shows the number density vs temperature calculated from constant pressure MD simulations using a Nose−Hoover thermostat. This liquid density was also confirmed by imaging the droplet and checking low-r level in the high-energy X-ray measurement oscillated about the theoretical limit. We estimate that there may be up to 5% error in this density value, which would produce up to a 5% error in the coordination numbers obtained.

4. RESULTS AND DISCUSSION

i. Neutron Structure Factors. The measured total structure factor for liquid $^{43}CaSiO_3$ is shown in Figures 4 and 5 together with the first order Ca-isotope difference function. A residual long wavelength background contribution to the Q-space total function was removed by setting the unphysical low-r oscillations to zero, and constraining the first Si−O Gaussian peak in real space to be consistent with tetrahedral coordination. This constraint was obtained from previous *in situ* X-ray measurements reported on molten $CaSiO_3$.[13] The first order difference function remained identical whether or

dx.doi.org/10.1021/jp3066019 | J. Phys. Chem. B 2012, 116, 13439−13447

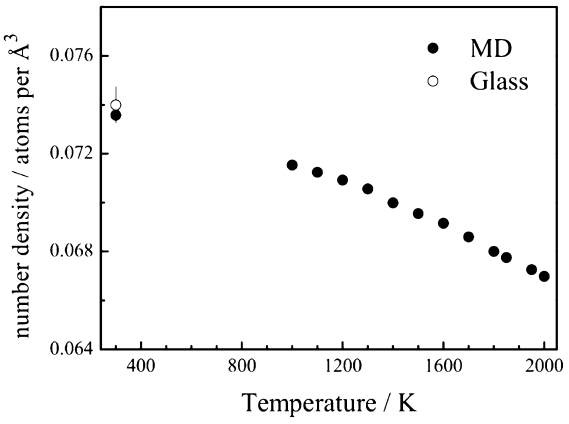

Figure 3. The black circles are the MD simulation density vs temperature points. The open circle is the glass density measurement. Note that the random error bars are too small to plot for the simulation points. Temperature steps between 700 and 300 °C were not calculated as the glass is already below its glass transition temperature at this point.

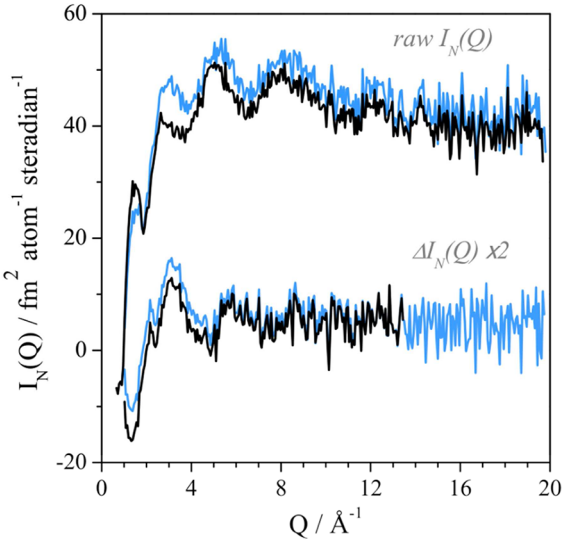

Figure 4. Measured differential neutron cross section for $CaSiO_3$ liquids. Top: raw total structure factors for liquid $CaSiO_3$. The blue line represents the natural sample and the black line is from the isotopically enriched sample. Bottom: difference structure factor for liquid $CaSiO_3$. The blue line is the raw difference data; the black line is the back-transformed data.

not this correction was imposed on the total structure factors, demonstrating that a difference technique is useful for extreme environments where absolute measurements can be problematic. The high accuracy of the experimental difference function was verified by the absence of the Si−O peak at 1.61 Å in $g(r)$; see Figure 2a. Both experimental functions $F_N(Q)$ for liquid $^{43}CaSiO_3$ and $F_N(Q)$ are in good agreement with published molecular dynamics simulations, see Figure 7.[13]

ii. Pair Distribution Functions. The measured total and isotopic neutron difference pair distribution functions for liquid $CaSiO_3$ are shown in Figure 6 together with the partial contributions from the MD model. The results are compared to a previously measured difference function on the glass[3] in Figure 7 with very similar partial neutron weighting factors. There is a dramatic decrease in the intensity of the first Ca−O bond peak in the liquid compared to the glass at 2.42 ± 0.02 Å.

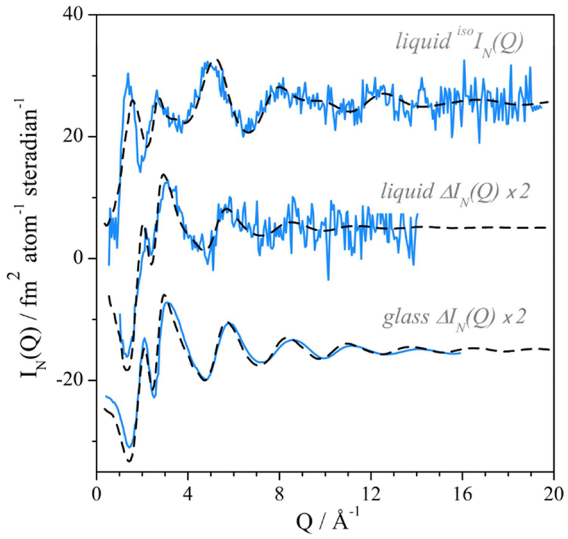

Figure 5. Solid blue lines: (top) the total neutron scattering, $I_N(Q)$ function for $^{43}CaSiO_3$ at 1650°C, (middle) the first order difference function at 1650°C, and (bottom) the first order difference function of the glass (data from[3]). The top and middle curves have been corrected imposing the constraint of SiO_4 tetrahedra, and back-transforming as described in the text. The black dashed lines are the results from molecular dynamics simulations on the liquid at 1727 °C and the glass at 27 °C using potentials from ref 13.

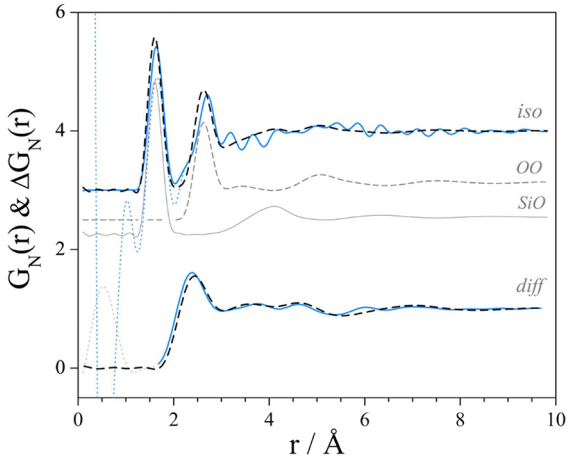

Figure 6. Pair distribution functions for liquid $CaSiO_3$ Top: Total pair distribution function of isotopic $CaSiO_3$. The black dashed line is the MD simulation, the blue dotted line is the transformed curve uncorrected at low-r and the solid blue line imposes the tetrahedral SiO_4 constraint and transformed with a Lorch modification function.[23] The gray lines are the MD generated O−O (dashed) and Si−O (solid), partials with the experimental weighting (these two partials make up over 90% of the total). Bottom: difference distribution function of liquid $CaSiO_3$. The experimental data transformed with a Lorch function is shown by the blue solid line and the MD simulation is the black dashed line. The gray dotted line at low-r represents the unphysical oscillations present in the difference measurement.

This decrease is concomitant with a broadening of the second and third peaks in $\Delta g(r)$ which are predominantly associated with the first neighbor Ca−Si and second nearest neighbor Si−O correlations based on the comparison with the MD results (also shown in Figure 8). Compared to previous structural models of the glass these observed changes are attributed to the distortion of predominantly CaO_6 polyhedra in the high

dx.doi.org/10.1021/jp3066019 | J. Phys. Chem. B 2012, 116, 13439−13447

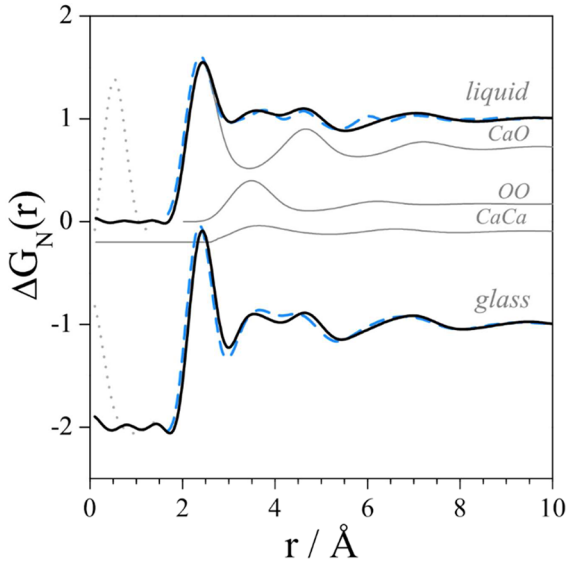

Figure 7. Top: measured difference pair distribution function, Δg(r), for liquid $CaSiO_3$ (dashed blue line) which contains only calcium correlations, compared to the neutron weighted MD partial structure (solid black line). Underneath the $\Delta g(r)$ are the contributing neutron weighted partial structure factors Ca−O, Ca−Si, and Ca−Ca from the MD simulation (thin gray lines) Bottom: previously measured, $\Delta g(r)$, for glassy $CaSiO_3$, data transformed from ref 4 (blue dashed line) compared to MD simulation curve (solid black line). All curves were Fourier transformed at the same Q_{max} = 10 $Å^{-1}$ with a Lorch modification function. The low-r unphysical oscillations of the measured data are plotted as gray dotted lines to distinguish them from the physical component of the measured data.

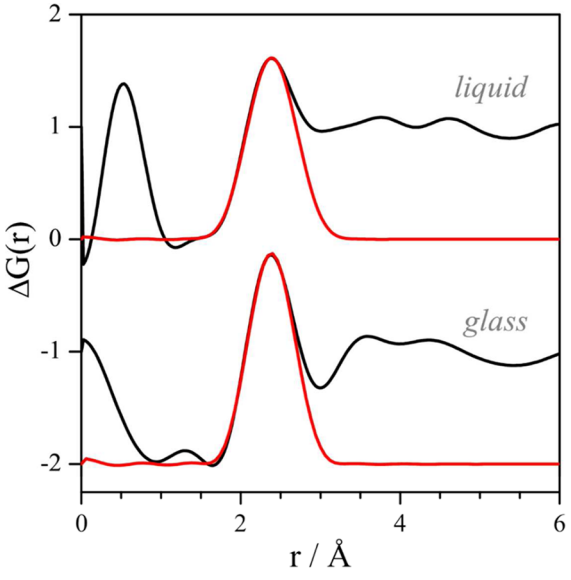

Figure 8. Measured $\Delta g(r)$ (black lines) and Gaussian coordination fits (red lines) for liquid and glassy $CaSiO_3$. The peaks were fitted to the low-r side of the measured Ca−O peaks. The fitted parameters are given in Table 3.

temperature melt.[3,8] The neutron results provide a rigorous test of previous MD simulations,[13] which predicted that the CaO environment broadens considerably in the melt compared to the glass.

iii. Ca−O Coordination Number. To determine the Ca−O coordination numbers in the liquid and glass fits were generated using the Q-space form of a Gaussian distribution of atom positions (see equation below), and Fourier transforming over the same Q-range as the first order difference data (Q-max =10 $Å^{-1}$). The symmetric peaks were fitted to the low-r side of the measured Ca−O peak (plotted in Figure 8).

$$P_1(Q) = \frac{w_{CaO}}{c_O} n_1 \sin(r_1 Q) \exp(-\sigma_1^2 Q^2/2) \quad (8)$$

Where w_{CaO} is the weighting of the Ca−O partial structure factor in $\Delta F_N(Q)$,n_1 is the coordination number of the peak, r_1 is the peak position, and σ_1 is the standard deviation. We note that Eckersley [7] reported a Ca−O coordination number of 6.15 ± 0.17 from their glass data, by intergrating up to the minimum beyond the first peak. The results of our analysis are shown in Table 3.

Table 3. Average CaO Coordination Number Peak Fit Parameters

	liquid	glass
position	2.43(2)	2.42(2)
CaO coordination	5.0(0.2)	6.0(0.2)
standard deviation	0.23(1)	0.195(5)
number density	0.067	0.074

Here we note that the glass studied by Gaskell et al. was not exactly $CaSiO_3$, but was $(CaO)_{48}(SiO2)_{49}(Al2O3)_3 \approx Ca_{0.87}Si_{0.89}Al_{0.11}O_{2.82}$, whereas due to evaporation, our recovered sample was 44.7 mol % SiO_2, i.e. $Ca_{1.24}Si_1O_{3.24}$. These are effectively opposite composition bounds of less modified (2.82 oxygen per network cation) and more modified (3.24 oxygen per network cation) compared to the $CaSiO_3$ composition. These changes in composition relative to $CaSiO_3$ are likely to affect the fraction of nonbridging oxygen in this system, and hence physical properties such as viscosity. To investigate the effect of this composition change on the Ca related structure (CaCa, CaSi, CaO partials) studied here we repeated our MD simulations using the Gaskell composition glass, and the composition of our recovered sample. Note that our measurment was the average of the $CaSiO_3$ starting composition and the $Ca_{1.24}Si_1O_{3.24}$ final composition over the 3 h measured (see also as section 2). Figure 9 compares the MD simulated Ca−O partial structure factors for the $Ca_{0.87}Si_{0.89}Al_{0.11}O_{2.82}$ (Gaskell), $CaSiO_3$, and $Ca_{1.24}Si_1O_{3.24}$ (recovered) composition liquids. From these $g_{CaO}(r)$ patterns we see only a very slight sharpening of the first Ca−O peak in the $Ca_{1.24}Si_1O_{3.24}$ liquid, and a very slight broadening in the $Ca_{0.87}Si_{0.89}Al_{0.11}O_{2.82}$ liquid, but no significant change in local coordination number, or overall Ca−O structure. This slight change in peak height is consistent with the more modified glass having less bridging oxygen and a slightly lower number density.

Figure 11 compares the Ca−O−Ca (interpolyhedral) and O−Ca−O (intrapolyhedral) bond angle distirbutions of the liquid and glass MD models. These have been divded by $\sin(\theta)$ to remove the effects of the finite sampling volume. These distributions provide information on the distortion and connectivity of the CaO units. A perfect octahedron for example will contain a single peak at an O−Ca−O angle of 90°, whereas the $CaSiO_3$ models both contain a broad main peak at 80° and an additional low angle peak around 55°. This significantly distorted unit is likely caused by the requirement of the Ca−O polyhedra to "fit into" the more strongly bound Si−O network. The Ca−O−Ca bond angle distribution however

dx.doi.org/10.1021/jp3066019 | J. Phys. Chem. B 2012, 116, 13439−13447

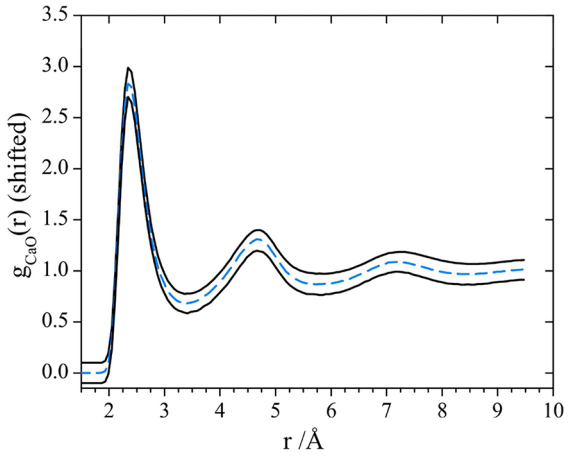

Figure 9. MD simulated CaO partial pair distribution functions for the three compositions each shifted vertically by 0.1. $Ca_{0.87}Si_{0.89}Al_{0.11}O_{2.82}$ (Gaskell composition, lower curve) $CaSiO_3$ (middle blue dashed curve) $Ca_{1.24}Si_1O_{3.24}$ (our recovered composition, upper curve). This plot shows only a very slight structural change in the CaO over this relatively small composition range. The number densities for these liquids at 1650 °C were 0.0681 (Gaskell), 0.0676 ($CaSiO_3$), and 0.0672 $Å^{-3}$ (recovered).

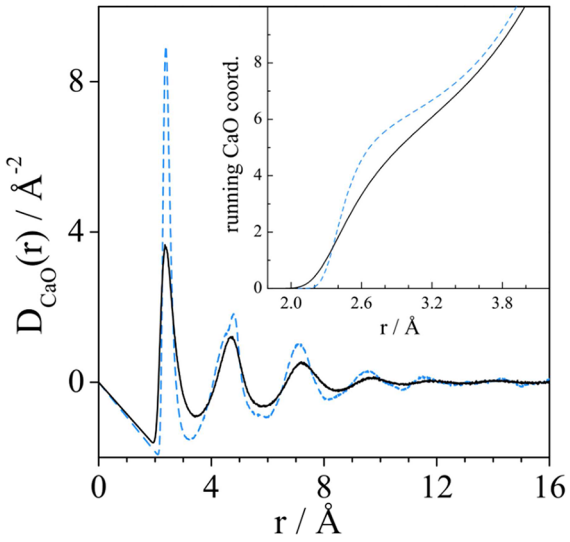

Figure 10. Ca–O partial distribution function, $D_{CaO}(r) = 4\pi\rho[g_{CaO}(r)-1]$ (see ref 21 for comparison to other definitions), for the liquid (black solid line) compared to the glass (blue dashed line) from the MD model (where ρ is the number density). The inset shows the running coordination number of the glass (blue dashed line) versus the liquid (black solid line).

provides information on the connectivty of CaO polyhedra. The Ca–O–Ca distribution of the MD model shows a main peak around 90°, which is the expected angle for edge sharing of neighboring CaO units. Between the liquid and glass models the 90° edge sharing peak, sharpens and increases in intensity, whereas the higher angle shoulder around 120° reduces between the liquid and glass models. These changes are explained by a decrease in the population of corner shared Ca–O–Ca connections (which occur at higher angles) and an increase edge-shared Ca–O polyhedra. This behavior is also reflected in direct analysis of the connectivity in these models as reported in.[13]

iv. Viscosity and Polymerization upon Cooling. Bockis and Lowe[20] measured the viscosity of calcium-silicate liquids and found that the activation energy exhibits a significant maximum at 52% CaO. The activation energies at >1700°C show a larger and smoother decrease with lime content than for <1700 °C. They[20] suggested the viscosity behavior could only be explained by discrete silicate ions or chains of silicate ions, and at the Ca_2SiO_4 (orthosilicate) composition the flow unit proposed was a 3-membered Si ring. Figure 12, which shows the relative proportions of Si–Si rings in our MD model, suggests that there are significantly more 3-membered rings in liquid $CaSiO_3$ compared to the glass, although they only represent a minor fraction (~7% in the liquid compared to ~1% in the glass). Moreover, our neutron first order difference, and MD results indicate that a large fraction of edge shared CaO_6 octahedra are also present in the melt. This excess of edge shared CaO_6, is also expected to increase viscosity and is consistent with the observation that this glass has an under-connected Si–O network.[26]

Since this composition has three oxygen atoms per silicon, the Si–O network has an average of 2 bridging oxygen per tetrahedron. The two bridging oxygen is less than the 2.4 connections per tetrahedron required by percolation theory for a rigid 3D network.[21] Hence in order for a glass to form at this composition, the Ca must be strengthening this weakly connected network. As such, we argue that Ca clustering is *required* for glass formation, and plays a significant role in increasing the viscosity of this liquid upon cooling. This clustering is in agreement with molecular dynamics simulations,[13] which suggest that although depolymerization of CaO_6 chains occurs in the melt compared to the glass, some nanometer scale heterogeneity still persists.

On the basis of the agreement of the MD study with the first order neutron difference data we suggest that the liquid at ~1650°C comprises of short chains of edge shared CaO_6, immersed in a corner shared SiO_4 network. The differences between the structural model of liquid $CaSiO_3$ compared to the model glass is illustrated by the MD Ca–O partial differential distribution functions (in Figure 10). These curves show a longer tail on the first Ca–O peak in the liquid state and the running coordination number shows a more disordered Ca–O coordination environment. The low field strength of the Ca^{2+} ion means that bonds can easily be distorted resulting in the disordered environment. Differences in chemical behavior of the group II metal silicates are clear from the phase diagrams for these systems. A detailed study of the effects of substituting different group II metals into the compositions would provide new insights into the effects of field strength on the structural evolution of the supercooled liquids.

5. CONCLUSION

We have extracted element specific cation interactions from a high temperature silicate melt, $CaSiO_3$, using neutron isotopic substitution on aerodynamically levitated droplets. Such information has recently proved impossible to extract using total scattering methods.[15] The *in situ* measurements provide detailed structural information on the Ca environment in the liquid state. Compared to similar experiments previously published on the glass, the liquid data show significant broadening of the Ca–O peak in the pair distribution function, which extends to longer distances in the melt. In addition, the first order Ca-neutron difference function is in good agreement with molecular dynamics simulations, which predict "channels"

dx.doi.org/10.1021/jp3066019 | J. Phys. Chem. B 2012, 116, 13439–13447

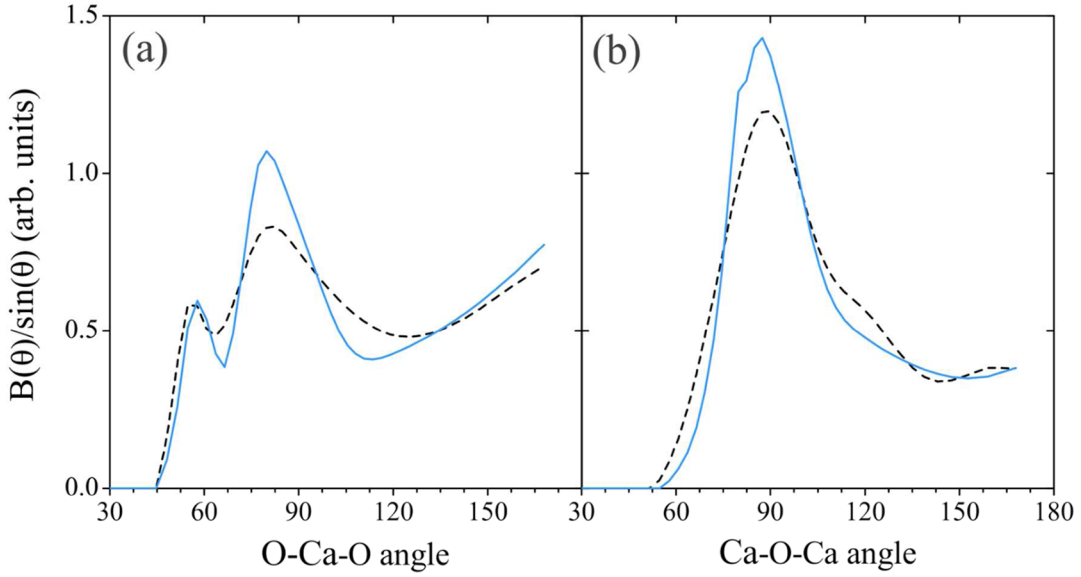

Figure 11. O−Ca−O (a) and Ca−O−Ca (b) bond angle distributions of the $CaSiO_3$ MD model at 1650 °C (black dashed line) and 300 °C (blue line). These were calculated up to CaO separations of 3.2 Å, which corresponds to the position of the minimum in $g_{CaO}(r)$.

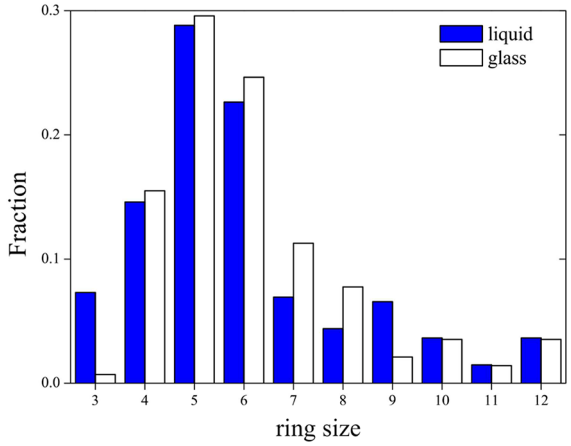

Figure 12. Ring statistics analysis of Si−Si−Si ring size distribution in $CaSiO_3$ liquid and glass. Calculated including separations up to 3.6 Å, which is close to the minimum in $g_{SiSi}(r)$. This shows a high fraction of low membered rings, with the most probable ring size of 5, which is significantly less than pure SiO_2 or GeO_2 glass which have near Gaussian ring size distributions centered between 6 and 7.

of mainly CaO_6 and CaO_7 polyhedra in the liquid.[8] It is anticipated that the development of this technique at high-flux neutron sources will yield detailed information on the structure of high temperature ceramics,[22] fragile liquids, and geologically relevant melts.[1]

AUTHOR INFORMATION

Notes

The authors declare no competing financial interest.

ACKNOWLEDGMENTS

We appreciate the efforts of Francis McCubbin and W. Woerner, for performing the probe analyses, and appreciate the access to infrastructure provided by H. Nekvasil and D. H. Lindsley at Stony Brook used for preparing the precursor materials for this study. We thank A. Pottebaum for developing the LabVIEW programs used to control the levitation experiments. This work was supported by the U.S. DOE under Phase I SBIR Grant Number 95612B10-1, at the Advanced Photon Source, Argonne National Laboratory under Contract Number DE-AC02-06CH11357, by NSF-DMR-0800415 (sample synthesis, microprobe analysis, and X-ray characterization), NSF-DMR-0907593 and DE-FG02-09ER46650 (support of LS and JBP at SNS and subsequent analysis). This Research at Oak Ridge National Laboratory's Spallation Neutron Source was sponsored by the Scientific User Facilities Division, Office of Basic Energy Sciences, U.S. Department of Energy. This research is also made possible by Oak Ridge National Laboratory contract DE-AC05-00OR22725.

REFERENCES

(1) Stebbins, J. F.; Farnan, I. *Science* **1992**, *255*, 586−589.
(2) Xue, X.; Kanzaki, M.; Tronnes, R. G.; Stebbins, J. F. *Science* **1989**, *245*, 962−964.
(3) Gaskell, P. H.; Eckersley, M. C.; Barnes, A. C.; Chieux, P. *Nature* **1991**, *350*, 675−677.
(4) Lee, S. K.; Stebbins, J. F. *J. Phys. Chem. B* **2003**, *107* (14), 3141−3148.
(5) Wilding, M. C.; Benmore, C. J.; Weber, J. K. R. *J. Phys. Chem. B* **2010**, *114* (17), 5742−5746.
(6) Lee, S. K.; Yi, Y. S.; Cody, G. D.; Mibe, K.; Fei, Y.; Mysen, B. O. *J. Phys. Chem. C* **2011**, *116* (3), 2183−2191.
(7) Eckersley, M. C.; Gaskell, P. H.; Barnes, A. C.; Chieux, P. *Nature* **1988**, *355*, 525−527.
(8) Mead, R. N.; Mountjoy, G. *J. Phys. Chem. B* **2006**, *110*, 14273−14278.
(9) Cristiglio, V.; Cuello, G. J.; Hennet, L.; Pozdnyakova, I.; Leydier, M.; Kozaily, J.; Fischer, H. E.; Johnson, M. R.; Price, D. L. *J. Non. Cryst. Solids* **2010**, *356*, 2492−2496.
(10) Kohara, S.; Itou, M.; Suzuya, K.; Inamura, Y.; Sakurai, Y.; Ohishi, Y.; Takata, M. *J. Phys.: Condens. Matter* **2007**, *19*, 506101.
(11) Landron, C.; Hennet, L.; Jenkins, T. E.; Greaves, G. N.; Coutures, J. P.; Soper, A. K. *Phys. Rev. Lett.* **2001**, *86*, 4839−4842.
(12) Mei, Q.; Benmore, C. J.; Weber, J. K. R. *Phys. Rev. Lett.* **2007**, *98*, 057802.
(13) Benmore, C. J.; Weber, J. K. R.; Wilding, M. C.; Du, J.; Parise, J. B. *Phys. Rev. B* **2010**, *82*, 224202.

(14) Wilding, M. C.; Benmore, C. J.; Weber, J. K. R. *Euro Phys. Lett.* **2010**, *89*, 26005.
(15) Drewitt, J.; Jahn, S.; Cristiglio, V.; Bytchkov, A.; Leydier, M.; Brassamin, S.; Fischer, H. E.; Hennet, L. *J. Phys.: Condens. Matter* **2011**, *23*, 155101.
(16) Fischer, H. E.; Barnes, A. C.; Salmon, P. S. *Rep. Prog. Phys.* **2006**, *69*, 233−299.
(17) Dianoux, A. J.; Lander, G. *ILL Neutron data booklet* 2nd ed.; OCP Science imprint: 2003 ISBN: 0-9704143-7-4.
(18) Nordine, P. C.; Weber, J. K. R.; Abadie, J. G. *Pure Appl. Chem.* **2000**, *72*, 2127−2136.
(19) Neuefeind, J.; Chipley, K. K.; Tulk, C. A.; Simonson, J. M.; Winokur, M. J. *Physica B* **2006**, *385*−*386*, 1066−1069.
(20) Bockris, J. O.; Lowe, D. C. *Proc. R. Soc. A* **1954**, *226*, 423−435.
(21) Boolchand, P.; Thorpe, M. F. *Phys. Rev. B* **1994**, *50* (14), 10366−10368.
(22) McMillan, P. F. *Nat. Mater.* **2008**, *7*, 843−844.
(23) Lorch, E. A. *J. Phys. C: Solid State Phys.* **1969**, *2*, 229−237.
(24) Weber, J. K. R.; Benmore, C. J.; Tangeman, J. A.; Siewenie, J.; Hiera, K. J. *J. Neutron Res.* **2003**, *11*, 113−122.
(25) Neuefeind, J.; Feygenson, M.; Carruth, J.; Hoffmann, R.; Chipley, K.K.. *Nuclear Instruments and Methods B* **2012**, *287*, 68−75.
(26) At the $CaSiO_3$ composition, there are on average only two bridging oxygen per tetrahedron. Here we are assuming a fully tetrahedral, corner shared SiO network is present with no significant non-network oxygen, and no triply connected or edge shared SiO tetrahedra.
(27) Hammersley, A. P.; Svensson, S. O.; Hanfland, M.; Fitch, A. N.; Hausermann, D. *High Press. Res.* **1996**, *14*, 235−248.
(28) Skinner, L. B.; Benmore, C. J.; Parise, J. B. *Nucl. Instrum. Methods A* **2012**, *662*, 61−70.